RESEARCH ARTICLE

NANO · MICRO small
www.small-journal.com

# Environment-Interactive Programmable Deformation of Electronically Innervated Synergistic Fluorescence-Color/Shape Changeable Hydrogel Actuators

*Junni Xie, Shuxin Wei, Wei Lu,* Shuangshuang Wu, Yi Zhang, Ruijia Wang, Ning Zhu,* and Tao Chen**

**Utilization of life-like hydrogels to replicate synergistic shape/color changeable behaviors of living organisms has been long envisaged to produce robust functional integrated soft actuators/robots. However, it remains challenging to construct such hydrogel systems with integrated functionality of remote, localized and environment-interactive control over synergistic discoloration/actuation. Herein, inspired by the evolution-optimized bioelectricity stimulus and multilayer structure of natural reptile skins, electronically innervated fluorescence-color switchable hydrogel actuating systems with bio-inspired multilayer structure comprising of responsive fluorescent hydrogel sheet and conductive Graphene/PDMS film with electrothermal effect is presented. Such rational structure enables remote control over synergistic fluorescence-color and shape changes of the systems via the cascading "electrical trigger-Joule heat generation-hydrogel shrinkage" mechanism. Consequently, local/sequential control of discoloration/actuation are achieved due to the highly controllable electrical stimulus in terms of amplitude and circuit design. Furthermore, by joint use with acoustic sensors, soft chameleon robots with unprecedented environment-interactive adaptation are demonstrated, which can intelligently sense environment signals to adjust their color/shape-changeable behaviors. This work opens previously unidentified avenues for functional integrated soft actuators/robots and will inspire life-like intelligent systems for versatile uses.**

## 1. Introduction

Many animals and plants in nature, like cephalopods,[1] chameleons,[2] apricot flowers,[3] are capable of synergistically adapting their color and shape in dynamic living environment for communication, camouflage, and intimidation.[4] Such marvelous phenomena have inspired scientists to merge the preferred color-changing capacity into soft actuators for producing ideal functional integrated soft robots (e.g., coexisting-cooperative-cognitive robots).[5] Over the past five years, a variety of color changeable soft actuators/robots were constructed based on polymeric hydrogels,[6] organohydrogels,[7] polymer films[5a,8] and biohybrid films.[9] Among them, polymeric hydrogels have received tremendous interest because of their hydrated soft wet nature, biotissue-like mechanical properties and good biocompatibility,[10] which makes synergistic color-shifting hydrogel actuators behave much more similar to living organisms and thus own great potential applications in soft robotics,[11] artificial muscles,[12] biosensors,[13] and microfluidic systems.[14] For instance, Tang et al.[15] designed an aggregation-induced emissive (AIE) hydrogel actuator showing synchronous variations in fluorescence color, brightness and shape in response to a single pH stimulus for frontier uses in the field of 3D/4D printing. We also have assembled the graphene oxide functionalized poly(N-isopropylacrylamide) hydrogel and pH-responsive perylene bisimide grafted hydrogel to fabricate an bilayer hydrogel actuator with synergistic "on–off" fluorescence response,[16] followed by further development of metal ions/solvent-responsive multicolor-fluorescence hydrogel actuators to better mimic the diverse discoloration behaviors of chameleons and octopi for biomimetic camouflage and disguise applications.[17] These advances have demonstrated the possibility of constructing biomimetic synergistic color/shape changeable hydrogel systems, and paved the way for the fabrication of robust functional integrated soft actuators/robots.

However, these coexisting synergistic color-shifting hydrogel actuators/robots are primarily chemically driven (e.g., acid/base,

J. Xie, S. Wei, W. Lu, S. Wu, Y. Zhang, R. Wang, T. Chen
Key Laboratory of Marine Materials and Related Technologies
Zhejiang Key Laboratory of Marine Materials and Protective Technologies
Ningbo Institute of Materials Technology and Engineering
Chinese Academy of Sciences
Ningbo 315201, P. R. China
E-mail: luwei@nimte.ac.cn; tao.chen@nimte.ac.cn
J. Xie, S. Wei, W. Lu, S. Wu, Y. Zhang, R. Wang, T. Chen
School of Chemical Sciences
University of Chinese Academy of Sciences
19A Yuquan Road, Beijing 100049, P. R. China
N. Zhu
College of Biotechnology and Pharmaceutical Engineering
Nanjing Tech University
Nanjing, Jiangsu 211800, P. R. China
E-mail: ningzhu@njtech.edu.cn

The ORCID identification number(s) for the author(s) of this article can be found under https://doi.org/10.1002/smll.202304204

DOI: 10.1002/smll.202304204

 

metal ions, solvent).[18] These classic chemical stimuli usually have difficulty in remote/localized control and thus cannot achieve the selective or sequential regulation of color/shape changes,[19] let alone to construct the environment-interactive hydrogel systems that can intelligently sense environment signals to adapt their color/shape changeable behaviors. This would hinder the performance of these actuators in complex tasks and hence impede the potential application. As a comparison, the chameleons have evolved to choose the remotely controllable bioelectricity stimulus as the trigger to regulate their skin colors and body gestures at all time in dynamic living environment. Interestingly, they also own the self-sensing capacity for environmental changes and then transmit nerve impulse (bioelectricity) to dictate the localized response behaviors, for example, to selectively regulate the synergistic color/shape changes of its certain part (e.g., the tail), while keeping the shape and skin color of other body parts unchanged.[20] These comparisons lead one to speculate that, if such natural electrical responsiveness was replicated, it would significantly enrich the intelligence and functional integration of artificial color-changing hydrogel actuators. On one hand, it is expected that localized and sequential control of discoloration/actuation will be guaranteed by the highly controlled electrical stimulus. On the other hand, compared with the classic chemical or thermal stimuli, the electrical stimulus can provide notable convenience for joint use with the existing acoustic/light sensors or change-over switches,[21] leading to one promising avenue that the wonderful environment-interactive adaptation of living organisms is unprecedentedly reproduced in artificial hydrogel actuators.

To replicate the electrically responsive color/shape changes in nature, it is essential to understand the evolution-optimized structure of soft wet reptile skin and the muscle beneath it as well as the bio-electrically innervated control mode. Recent anatomical and biological studies revealed the vertically arranged multilayer structure of chameleon skins, in which each layer is composed of different-colored pigment cells around with a ring of innervated muscular cells[2,20a] (**Scheme 1**a). Upon reception of environmental changes, nerve impulse (bioelectricity) was generated and transmitted to induce muscular movement for modulating the differential dispersion/aggregation of these pigment cells, thereby causing the local skin color change. Meanwhile, nerve impulse was also precisely delivered to dictate localized deformation of muscle tissues beneath the skin. In this way, selective and spatial control over synergistic shape/color changeable behaviors are accomplished owing to such rational multilayer structure design of natural reptiles that facilitates efficient functional synergy of soft wet skin and muscle bio-issues. Inspired from this, we have recently developed a series of multicolor fluorescent polymeric gels[22] and assembled them with soft electrothermal materials to produce electrically-controlled fluorescence-color changing polymeric gel systems for camouflage and information display applications.[18,23] However, because of the weak supramolecular interactions between polymer gel and soft electrothermal layer in these systems, they failed to achieve the biomimetic electrically-controlled synergistic fluorescence-color/shape changeable hydrogel actuators, let alone to achieve the selective or sequential regulation of color/shape changes and the environment-interactive hydrogel systems that can intelligently sense environment signals to adapt their color/shape changeable behaviors.

Herein, by further learning from the bioelectricity stimulus and rational multilayer interlocking skin structure of natural reptiles, we elaborately design electrically innervated synergistic fluorescence-color/shape changeable hydrogel (ECC) actuators. As schemed in Scheme 1b, the ECC actuators were specially designed to have the reptile skin-like multilayer structure consisting of the fluorescence-color changeable poly(HEMA-DMAEMA-DAEAN-DEAN) (PH3D) hydrogel sheet and conductive Graphene/PDMS thin film that were bonded together by one flexible adhesive layer via strong covalent and hydrogen-bonded interactions.

The PH3D hydrogel consists of AIE-active blue-light-emitting DAEAN fluorogens and chartreuse-light-emitting DEAN fluorogens, as well as electron-rich tertiary amine group of copolymerized 2-(Dimethylamino)ethyl methacrylate (DMAEMA) moieties, which allow competition between PET (photoinduced electron transfer) effect from DMAEMA to fluorogens, and AIE effect of fluorogens during dehydration process. This competition would result in blue-to-chartreuse fluorescence color change. In this way, upon applying voltage to the graphene film, Joule heat was instantly generated and transferred across PDMS to induce the shrinking of PH3D hydrogel, leading to the simultaneous blue-to-chartreuse fluorescence color change and shape deformation of ECC actuator (Scheme 1c). Owing to the highly controllable electrical stimulus in terms of magnitude and circuit design, the electrically innervated ECC actuators further enabled the joint use with existing change-over switches and acoustic sensors, producing soft chameleon robots with selective and spatial control over color/shape changes, as well as environment-interactive adaptation (Scheme 1d).

## 2. Results and Discussion

### 2.1. Preparation of the Fluorescence-Color Changeable Hydrogels

The fluorescence color changeable poly(HEMA-DMAEMA-DAEAN-DEAN) (PH3D) hydrogel was prepared by a thermally induced free radical copolymerization of 2-hydroxyethyl methacrylate (HEMA), 2-(dimethylamino)ethyl methacrylate (DMAEMA) and a small quantity of Bis crosslinker, as well as two fluorescent monomers, 4-(2-dimethylaminoethyloxy)-N-allyl-1,8-naphthalimide (DAEAN) and 4-(*N,N*-dimethylaminoethylene) amino-N-allyl-1,8-naphthalimide (DEAN) (Figures S1,S2 and Note S1, Supporting Information). These two randomly copolymerized AIE-active DAEAN and DEAN fluorophores are known to be blue- (≈442 nm) and chartreuse-light emitting (≈520 nm), respectively (Figure S3, Supporting Information). Notably, copolymerized DMAEMA moieties have electron-donating tertiary amine groups, which were known to show potential photoinduced electron transfer (PET) process to quench the fluorescence of these two fluorophores (DAEAN and DEAN).[24] Nevertheless, the tertiary amine groups of the copolymerized DMAEMA moieties could be protonated in acidic environment, thus endowing the as-prepared PH3D hydrogel with controllable swelling behaviors in aqueous $CO_2$ solution and meanwhile hindering the PET process between DMAEMA and fluorophores.[25] Consequently, the reversible fluorescence-color changes were

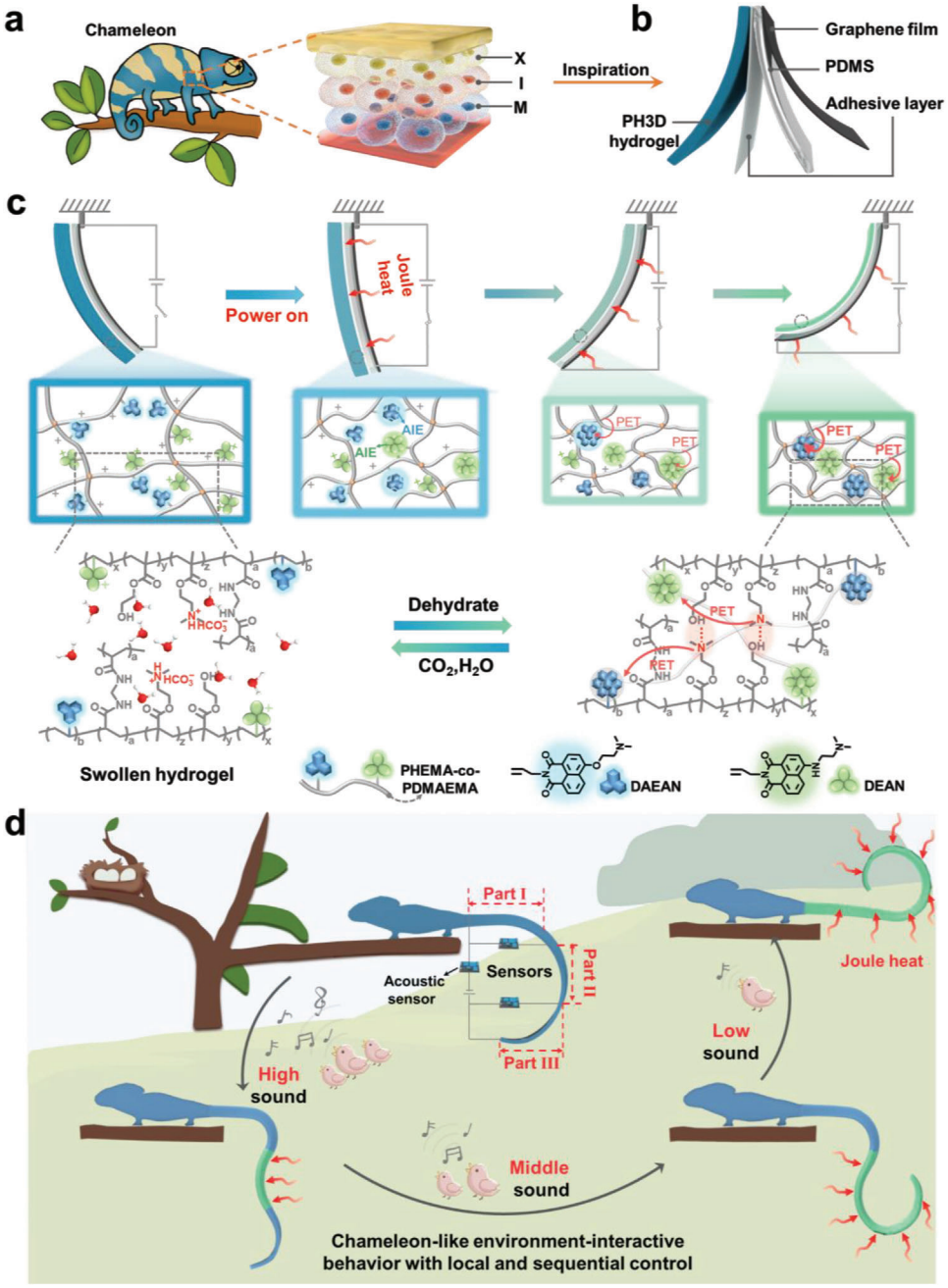


**Scheme 1.** Design of bioinspired electrically-powered hydrogel actuators with synchronous fluorescence-color and shape changing ability. a) Illustration showing the vertical multilayer arrangement of several chromatophores (X, I, and M denote Xanthophore, Iridophores, and Melanophore) in chameleon skin. b) Illustration of the ECC actuator with bio-inspired multilayer structure. c) Illustration showing the synergistic fluorescence-color and shape changing process of the ECC actuator, as well as the proposed mechanism for fluorescence color changes. d) Illustration of an environment-interactive artificial chameleon actuator capable of selectively adjusting its skin color and body shape upon the reception of different-decibel sound signals.

observed as its $CO_2$-induced swelling/heat-triggered deswelling proceeded. As can be seen from **Figure 1**a–d, the as-prepared $PH3D_0$ hydrogel with 97.53% water content exhibited only one emission band ≈442 nm when excited at 365 nm and was thus blue-light emitting. This is possibly because protonated DEAN moieties can not tend to aggregate in $PH3D_0$ due to electrostatic repulsion, thus leading to weak chartreuse fluorescence intensity. When placed at 80 °C for 1 min to enable partial water evaporation, the $PH3D_1$ hydrogel with 91.77% water content was obtained. Interestingly, its emission peak at 520 and 442 nm was noticeably enhanced (1.64-fold and 1.47-fold), suggesting the increased concentration and aggregation-induced emission enhancement (AIE effect) of these AIE-active fluorophores induced by dehydration (Stage I) (Figure 1c,d). After that, the copolymerized DMAEMA moieties were gradually deprotonated owing to the evaporation of $CO_2$. As a result, the well-known

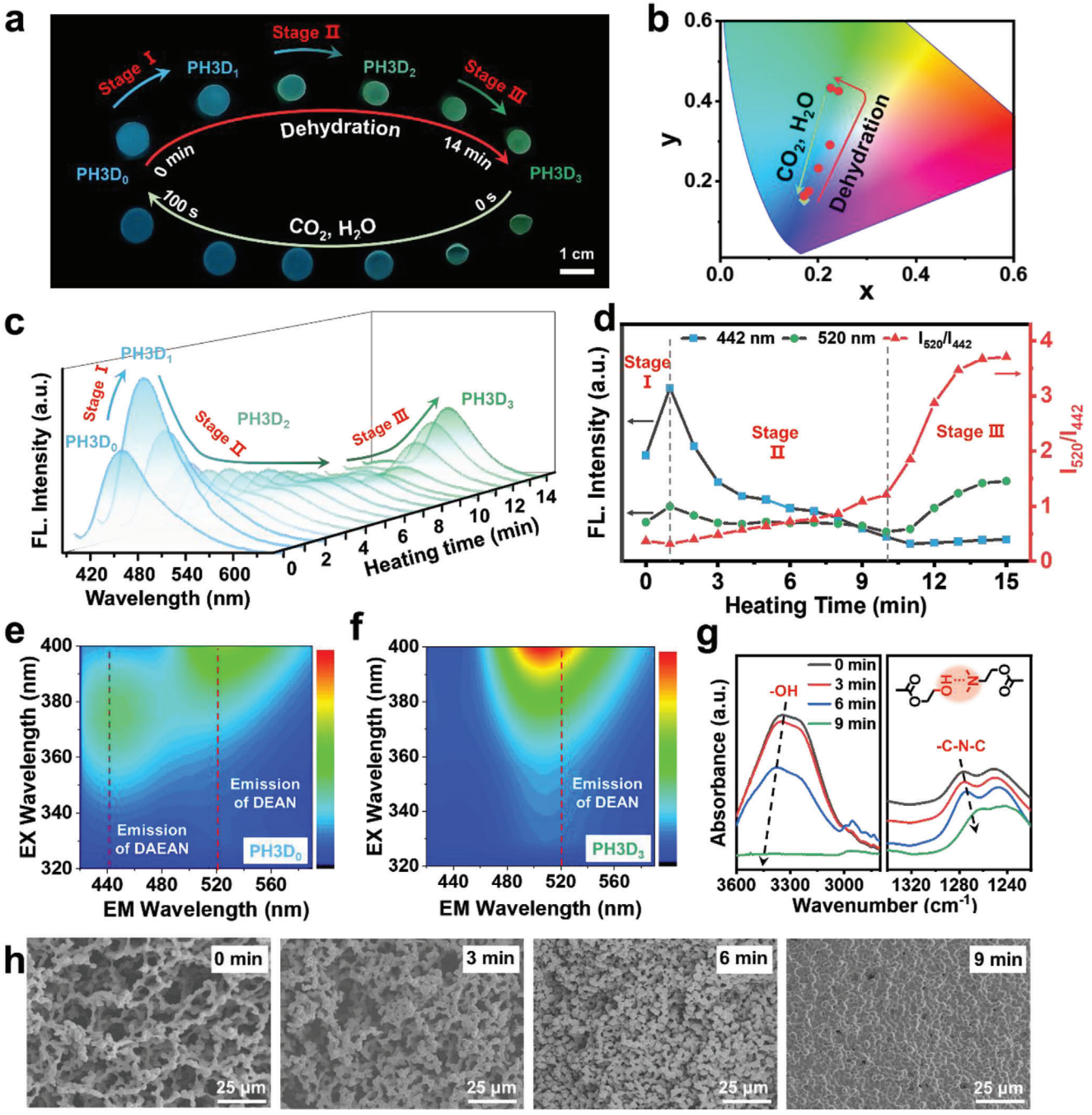


**Figure 1.** Fluorescence-color switchable PH3D hydrogel. a) Photos of PH3D hydrogel taken during the dehydrated process (heated at 80 °C for 14 min) and re-swelling process (immersed to saturated aqueous $CO_2$ solution for 100 s) under a 365 nm UV lamp. b) CIE (1931) coordinate diagrams of these dehydrated and re-swollen PH3D hydrogels. c) Fluorescence spectra ($\lambda_{ex}$ = 365 nm) of $PH3D_0$ hydrogels that were recorded at different time intervals after being heated at 80 °C. d) Fluorescence intensity at 442 and 520 nm, as well as intensity ratio at 520 to 442 nm as function of heating time. e,f) 3D-fluorescence spectra ($\lambda_{ex}$ from 320 to 400 nm, $\lambda_{em}$ from 420 to 570 nm) of $PH3D_0$ (e) and $PH3D_3$ (f) hydrogels. g,h) FT-IR spectra (g) and SEM (h) images of these freeze-dried $PH3D_0$ hydrogels after being heated (80 °C) at different time intervals.

photoinduced electron transfer (PET) between these fluorophores and deprotonated dimethyl amino groups was activated (Stage II). At this stage II, it seemed that the PET effect overwhelmed the AIE effect, thus leading to the gradual fluorescence quenching (Figures S4,S5 and Notes 2,3, Supporting Information). Interestingly, the chartreuse intensity of PH3D hydrogel was further enhanced after 10 min (Stage III), suggesting that the AIE effect further overwhelmed the PET effect possibly due to the fact that most water had been evaporated from the PH3D hydrogel. Nevertheless, the blue intensity of PH3D

hydrogel was not enhanced at this Stage III. To elucidate this interesting phenomenon, additional four polymer gels were prepared (Figure S6, Supporting Information) and subject to systematical photophysical studies. As shown in Figure S7 (Supporting Information), it was found that PDMAEMA matrix showed strong PET effect for both DAEAN and DEAN fluorophores (Figure S7a–c, Supporting Information), while PHEMA matrix showed selective fluorescence quenching for the DAEAN fluorophore (Figure S7d–f, Supporting Information). This new finding may explain why only the chartreuse intensity of DEAN fluorophore was enhanced at Stage III. More evidences for the fluorescence-color variation of $PH3D_0$ hydrogel before and after dehydration were deduced from the excitation-fluorescence mapping measurements of $PH3D_0$ and $PH3D_3$ hydrogels. As shown in Figure 1e, $PH3D_0$ has two emission bands ≈442 and 520 nm under excitation at 365 nm. After being dehydrated to $PH3D_3$, its blue emission band ≈442 nm disappeared accompanying with dramatically enhanced chartreuse emission band ≈520 nm, indicating that fully quenched blue fluorescence and remarkably increased chartreuse fluorescence after dehydration. These results are consistent with the steady state fluorescence spectra shown in Figure 1c. Importantly, the dehydrated chartreuse-light-emitting $PH3D_3$ (13.04% water content) hydrogel would fully recover to its initially swollen state ($PH3D_0$) with blue fluorescence after being immersed in aqueous $CO_2$ solution for 100 s (Figure 1a,b). To further elucidate this fluorescence-color changing mechanism, time-dependent Fourier transform infrared (FT-IR) studies were carried out. In Figure 1g and Figure S8 (Supporting Information), the stretching bands at 3345 and 1633 $cm^{-1}$ responding to the -OH groups and H-bond C = O groups exhibited a blue-shift upon increasing heat time, accompanied by the intensity reduction of these peaks.[26] Meanwhile, the bands at 2956, 2840 $cm^{-1}$ related to stretching vibrations of C-H groups were shifted to lower wavenumbers[27] (Figure S5, Supporting Information). These results indicate the dissociation of hydrogen bonds between PH3D and water molecules as the result of water evaporation. Importantly, the characteristic band of C—N—C bond (≈1280 $cm^{-1}$) of PH3D was shifted to a lower wavenumber as the heating time increased (Figure 1g), representing the formation of hydrogen bonds between the tertiary amine and hydroxyl groups.[28] Besides, an increased absorption in the visible light region was observed, indicating the gradual aggregation of polymer chains (Figure S9, Supporting Information). More direct evidences came from the cross-section surface morphologies of these freeze-dried PH3D hydrogels that were recorded at different time intervals during the heating process at 80 °C. As shown in Figure 1h, their SEM images demonstrated that the polymer chains were indeed brought into closer proximity with prolonging heating time, which was in favor to activate the AIE process of DEAN fluorogens, thus inducing blue-to-chartreuse fluorescence color change.

### 2.2. Fabrication of Electrothermal Synergistic Fluorescence-Color Changeable Soft Actuator

Electrically controlled fluorescence color-changeable (ECC) soft actuators were then prepared by interfacially assembling the responsive fluorescence-color changeable PH3D hydrogel sheet and conductive Graphene/PDMS thin film. As illustrated in Figure S10a (Supporting Information), Graphene/PDMS film was first obtained by transferring the stacked graphene assembly (SGA) at water-air interface onto thin PDMS substrate (≈200 μm).[29] For ensuring the stable interfacial bonding between PH3D hydrogel and Graphene/PDMS film, an adhesive polymer layer containing acrylic acid-N-succinimide ester (AAc-NHS-ester) was specially designed and grown on the PDMS surface according to an interfacial polymerization method inspired by the previous studies[30] (Figure S10b, Supporting Information). Then, the ECC actuator could be facilely prepared, whose interfacial multilayer structure was clearly depicted in the cross-section SEM images. It was found that the PH3D hydrogel sheet and conductive Graphene/PDMS thin film were closely glued together by the adhesive polymer layer (**Figure 2**a; Figure S11a,b, Supporting Information). FT-IR studies of this middle adhesive layer suggested that the C-N-C stretching peak at 1321 $cm^{-1}$ associated to NHS ester moiety vanished, signifying its successful covalent bonding with the PH3D hydrogel sheet via the esterification reaction shown in Figure S12 (Supporting Information).[30a] Meanwhile, the stretching vibration peak of -OH (≈3400 $cm^{-1}$) red shifted to a lower wavenumber, further indicating the enhanced hydrogen bonds between the PH3D hydrogel sheet and middle adhesive layer. As such, the ECC actuators with stable interlocking multilayer structures were obtained, which supplied an excellent basis for further actuating studies.

Working principle of the ECC actuators with one end fixed was then studied. As illustrated in Figure 2b, when applying voltage on its graphene film layer, Joule heat was generated owing to electrocaloric effect and instantly transferred across PDMS to the swollen PH3D hydrogel layer, resulting in gradual dehydration and shrinking of the hydrogel layer. Consequently, the free end of this ECC actuator would gradually bend toward the hydrogel layer, accompanying with a distinct blue-to-chartreuse fluorescence color change. In this way, the electro-thermally powered synergistic shape and fluorescence color changeable behaviors were realized. Due to the highly controlled electrical stimuli in terms of amplitude and duration, the surface temperature on Graphene /PDMS film could be accurately adjusted by facilely varying the thickness of graphene film, magnitude of voltage or power-on time, providing solid foundation for precisely and remotely regulating such synergistic actuating performances[18] (Figure 2c; Figures S13–16a, Surppoting Information). As compared in Figure 2d and Figure S16b (Supporting Information), there was nearly no bending deformation within the first 4 min after applying 6, 12, and 15 V voltage, while a large bending movement was observed for the free end under the input of 20 V. Also, much larger bending deformation was observed at 8 min for the ECC actuator with 20 V input. This is because larger voltage input was known to generate more Joule heat within the same duration time. This speculation was consistent with the recorded surface temperatures of these actuators (Figure S17, Supporting Information), which indicated that the surface temperature quickly reached ≈120 °C within 4 min at 20 V and was much higher than that recorded at 12 V or 15 V (≈45 °C). To quantitate such voltage-dependent actuating processes, their bending angles as a function of time were summarized in Figure 2e and Figure S16c (Supporting Information). Obviously, both the actuating extent and speed of the ECC actuators were in positive

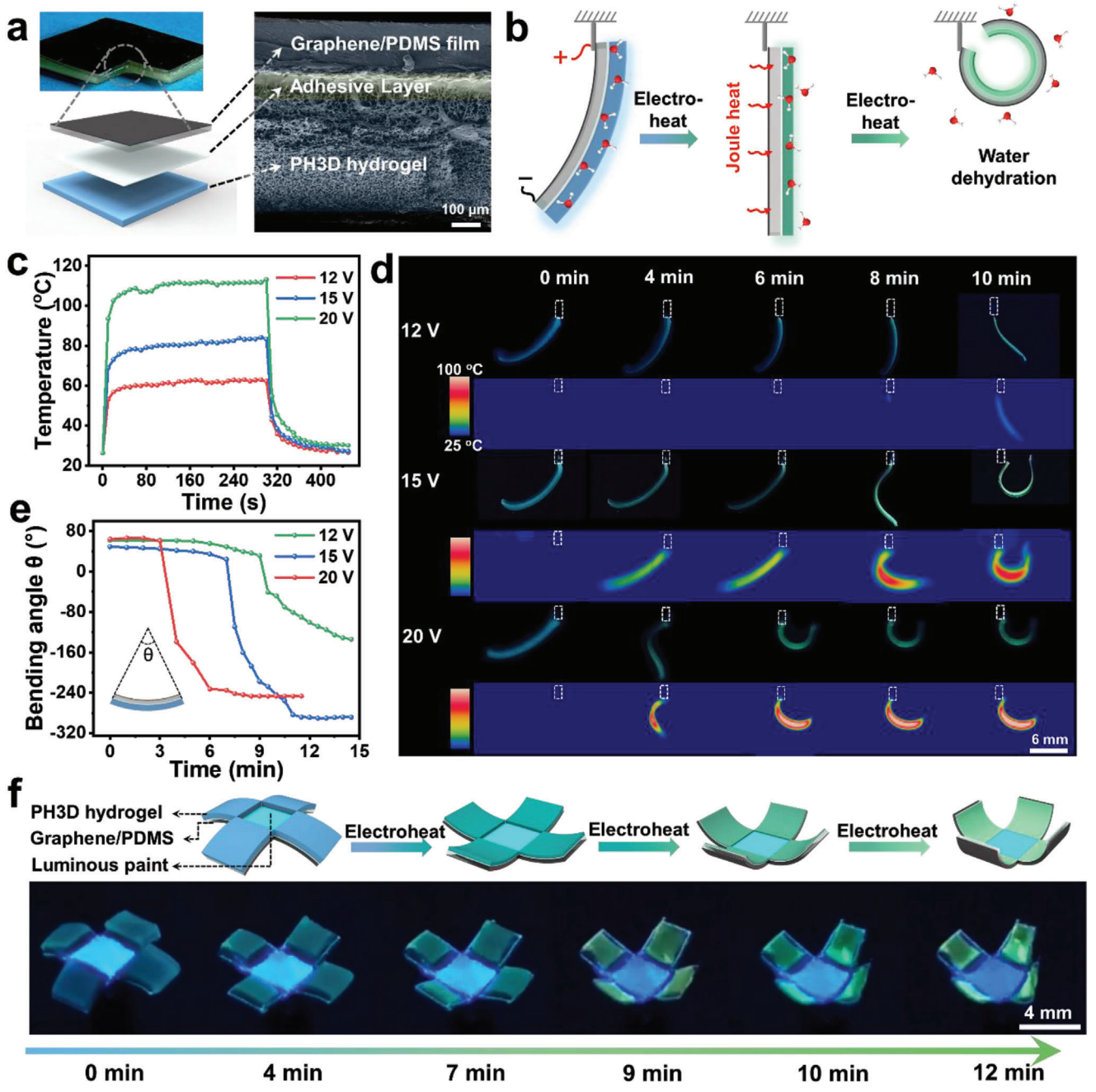


**Figure 2.** Structure and working principle of the ECC actuators. a) Photo, Illustration and cross-section SEM image of the actuator. b) Illustration showing the electro-thermally powered actuating process of the ECC actuator with one end fixed. c) Temperature recorded on the Graphene/PDMS film as a function of the power-on time. d) Photos taken under a 365 nm lamp and corresponding IR images showing the electrically controlled fluorescent color/shape changeable process of the actuator under the input of different voltage. e) Bending angle $\theta$ of these actuators as a function of the power-on time at different voltages. f) Illustration and photos showing the structure and time-dependent actuating process of a cruciform ECC actuator under the input of 15 V voltage.

correlation with the magnitude of input voltage, verifying the high adjustability of electrical stimulus. As a comparison, the synergistic shape/color changes of this actuator induced by natural water evaporation was characterized at room temperature (≈27 °C). As shown in Figure S18 (Supporting Information), this actuator could keep good stability within 30 min, but began to actuate after 35 min. Interestingly, the bending angle was found to change nearly linearly with time. Meanwhile, noticeable blue-to-green emission color changes were observed (Figure S19, Supporting Information). Compared with the electrothermally powered actuators (Figure 2d), the actuating behavior induced by natural water evaporation at room temperature was much slower because of the relatively slow water evaporation. Remarkably, the electrically powered synergistic shape and fluorescence

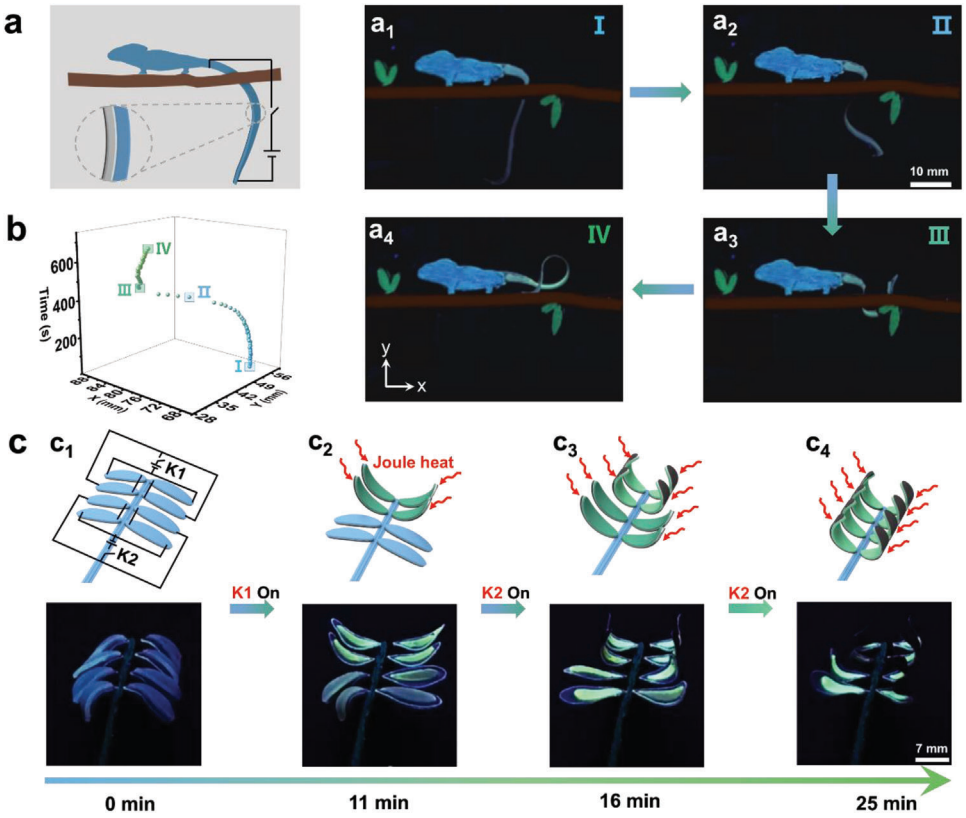


**Figure 3.** Demonstration of bionic leaf-like ECC actuators. a,b) Photos showing the time-dependent deformation of the chameleon-like actuator under the input of 15 V voltage (a) and the motion trajectory of its tail end (b). c) Illustration and the corresponding photos taken under the input of 5 V voltage showing the electrically powered stepwise color/shape changes of Mimosa-like actuator. All photos were taken under a 365 nm UV lamp.

color changes could be fully reversed by further immersing the ECC actuators into $CO_2$ aqueous solution for 4 min (Figure S20. Supporting Information). Further investigations suggested that such reversible actuating processes triggered by sequential electric and $CO_2$ stimuli could be held for at least 6 cycles (Figure S21, Supporting Information) without significant performance loss.

Considering the facile operation of the proposed interfacial assembly strategy, a variety of electrically powered actuators with customized shapes could be easily constructed. As a typical example, one cruciform actuator was fabricated according to the structure design in Figure 2f. In this design, the non-responsive blue luminous paint was placed in the middle area for serving as the control to facilitate the observation of fluorescence color changes in the hydrogel layer. The obtained actuator initially curled downward with a blue fluorescence, but gradually flattened after applying voltage (15 V) for 4 min, and finally curled upward along with a noticeable blue-to- chartreuse fluorescence color change after prolonging the power-on time to 12 min (Movie S1, Supporting Information). Following a similar way, one non-centrosymmetric cruciform actuator was constructed and exhibited an analogous movement mode (Figure S22, Supporting Information). Interestingly, one spiral actuator also could be fabricated through assembling PH3D hydrogel strips to Graphene/PDMS film at 45 degrees and gradually untied the spiral into straight strip upon applying 15 V voltage (Figure S23, Supporting Information).

### 2.3. ECC-Based Bionic Actuators

Many natural animals and plants show interesting shape changes for better adaption to dynamic living environment. For example, chameleons have evolved to exhibit responsive body shape and skin color changes for communication, camouflage and intimidation. To mimic this interesting behavior, we constructed a hydrogel chameleon by using a stripe-shaped ECC actuator as the tail to integrate with the luminous paint body, whose structure and control circuit were illustrated in **Figure 3**a and Figure S24 (Supporting Information). As expected, upon applying 15 V voltage, its tail gradually and continuously curled up with increasing power-on time. The trajectory of the end tail of this chameleon was summarized in Figure 3b. Notably, this shape-deformation process was accompanied with a visible emission color change from blue to chartreuse (Movie S2, Supporting Information).

In addition to animals, tree leaves can wilt/curl at high temperature to prevent collapse. This intriguing behavior of natural tree leaves inspired us to develop their artificial counterparts. As depicted in Figure S25 (Supporting Information), one bionic tree was prepared by tethering several leaf-like ECC actuators onto its branches, in which each leaf was connected with a circuit. After applying a driving voltage of 10 V, these leaves gradually curled over time due to the shrinking of PH3D hydrogel layer induced by Joule heat of the graphene film beneath (Movie S3,

Supporting Information). Taking the leaf indicated by a red circle in Figure S25 (Supporting Information) as an example, it exhibited slight shape deformation within the initial 2.5 min when the temperature was not high enough. But rapid curling upwards into the wilting state was subsequently observed, as evidenced by the motion trajectory in Figure S26 (Supporting Information). Besides tree leaves, artificial Mimosa that can sequentially fold up its leaves for self-defense against environmental interferences has also been demonstrated by attaching eight leaf-like ECC actuators to the same plastic stem. Figure 3c depicts its circuit design which contained two individual switches (K1 and K2) to control the upper four leaf-like actuators and the lower four ones, respectively. When switch K1 was turned on to generate Joule heat, the upper four leaves would be folded up (Figure $3c_{1,2}$). Subsequently, the other four leaves would be triggered to gradually close after turning on switch K2 (Figure $3c_{3,4}$). In this way, the unique sequential closure behavior of Mimosa leaves was fully replicated in our electrically powered artificial systems by remotely and facilely varying the electrical stimulus (Movie S4, Supporting Information).

### 2.4. ECC Actuators with Local and Sequential Control Over Shape/Color Changes for Environment-Interactive Adaptation

Soft actuators with such local and sequential shape/color control hold great potential to perform complex tasks, but have hardly been achieved owing to the difficulty in precise manipulation of such traditional stimuli as pH or metal ions. Benefiting from the highly controllable electrical stimulus in terms of amplitude and duration, as well as its natural compatibility with the commercial electric devices, we herein demonstrated one such example through the joint use of our electrically powered synergistic shape/color changeable actuator and a commercial universal change-over switch (UCOS). **Figure 4**a depicted the designed system and its customized circuit design. This stripe actuator with one end fixed was equipped with four evenly distributed electrodes that were connected with one specially designed UCOS. Specifically, when the UCOS turned to switch 1, the graphene film beneath part I of the actuator was powered on to generate the local Joule heat, which selectively induced the simultaneous bending deformation and blue-to-chartreuse fluorescence color change of Part I (Figure $4a_{1\text{-}2}$, $b_{1\text{-}2}$). Following a similar line, the graphene film beneath part III and part II could be powered on successively by shifting the UCOS to switch 2 and 0 in sequence. Consequently, synergistic color/shape changeable behaviors were observed first for part III and then part II of the designed actuator (Figure $4a_3$,$a_4$, $b_3$–$b_5$). Three distinct motion trajectories after triggering Switch 1, 2 and 0 was summarized in Figure 4c. In this way, the preferred sequential actuating behaviors were achieved by facilely varying the power-on sequence of the UCOS circuit (Movie S5, Supporting Information).

One key differentiator between biological and artificial systems is the environment-interactive actuating performances of living organisms, enabling the self-sensing of external environment changes to intelligently regulate their actuating states for better adaption to dynamic living environments. Compared with the existing hydrogel actuators that were controlled by traditional stimuli such as ions or acid/base, the proposed electrical stimulus provides notable convenience for joint use with the commercial sensors, thus holding great potential to produce conceptually new environment-interactive artificial actuators. To show this potential, acoustic sensors were specially utilized to automatically control the power on/off of our ECC actuators, an environment-interactive artificial chameleon actuator with locally and sequentially controllable ability was herein constructed, which could better resemble the natural chameleon to adjust the actuating behaviors of its tail part. Figure 4d shows the customized circuit of this artificial chameleon, in which three acoustic sensors with different sensitivity were delicately utilized to intelligently control the power-on/off of Part I, II, and III in the tail actuator, respectively. At normal conditions, all of these three switches were powered off to let the chameleon naturally drop its tail (Figure $4d_1$). But at a sudden great noise, all of these three switches would be activated to apply voltage (20 V) onto the graphene film beneath part II of the tail. Consequently, local Joule heat was immediately generated to induce the synchronous bending deformation and blue-to-chartreuse fluorescence color change of Part II (Figure $4d_2$). With the environment sound gradually got down, VOX3 switch with the lowest sensitivity was first turned off to successively connect the graphene films beneath Part II and III into the circuit, leading to the sequential shape/color changes of Part III (Figure $4d_3$). With further decrease of the environment sounds, synchronous shape/color changeable behavior of part I would be finally observed. This is because only the most sensitive VOX1 switch was kept on to make the graphene film beneath the whole chameleon tail generate Joule heat (Figure $4d_4$). Figure S27 (Supporting Information) shows more detailed information of this environment-interactive programmable actuation behavior. Notably, as shown in Figure 4e, this environment-interactive chameleon with locally and sequentially controllable ability has the more complicated motion trajectory than that common one shown in Figure 3b. In this way, the robust artificial chameleon with life-like environment-interactive sequential actuating behaviors was demonstrated for the first time based on our electrically powered ECC actuator (Movie S6, Supporting Information). In addition, an environment-interactive system containing leaves and different chameleons was demonstrated by specially utilizing acoustic sensors to automatically control the power on/off of different shaped ECC actuators. The schematic circuit of this system and corresponding pre-set program within acoustic sensors were shown in Figures S28 and S29 (Supporting Information). As the example shown in **Figure 5**a exhibited, the four leaf-like actuators in the background tree branch were connected with a highly sensitive acoustic sensor VOX1, and the tail actuators of these two chameleons were controlled by the acoustic sensor VOX2 and VOX3 with middle and lowest sensitivity, respectively. At normal decibel, all of these three switches were turned off to ensure that these two chameleons naturally dropped their tails and the four leaves kept the stretching state. When the surrounding sound slightly increased to activate the VOX1 sensor, the graphene films beneath these four leaves would be powered on to generate Joule heat, which induced the bending deformation of these leaves. Interestingly, the two small leaves with bigger resistance bended before those two big ones as a result of more Joule heat according to Joule's law ($Q = I^2Rt$) (Figure 5b). With increasing environment-sound decibel, the VOX2 switch with middle sensitivity was subsequently powered on to activate the

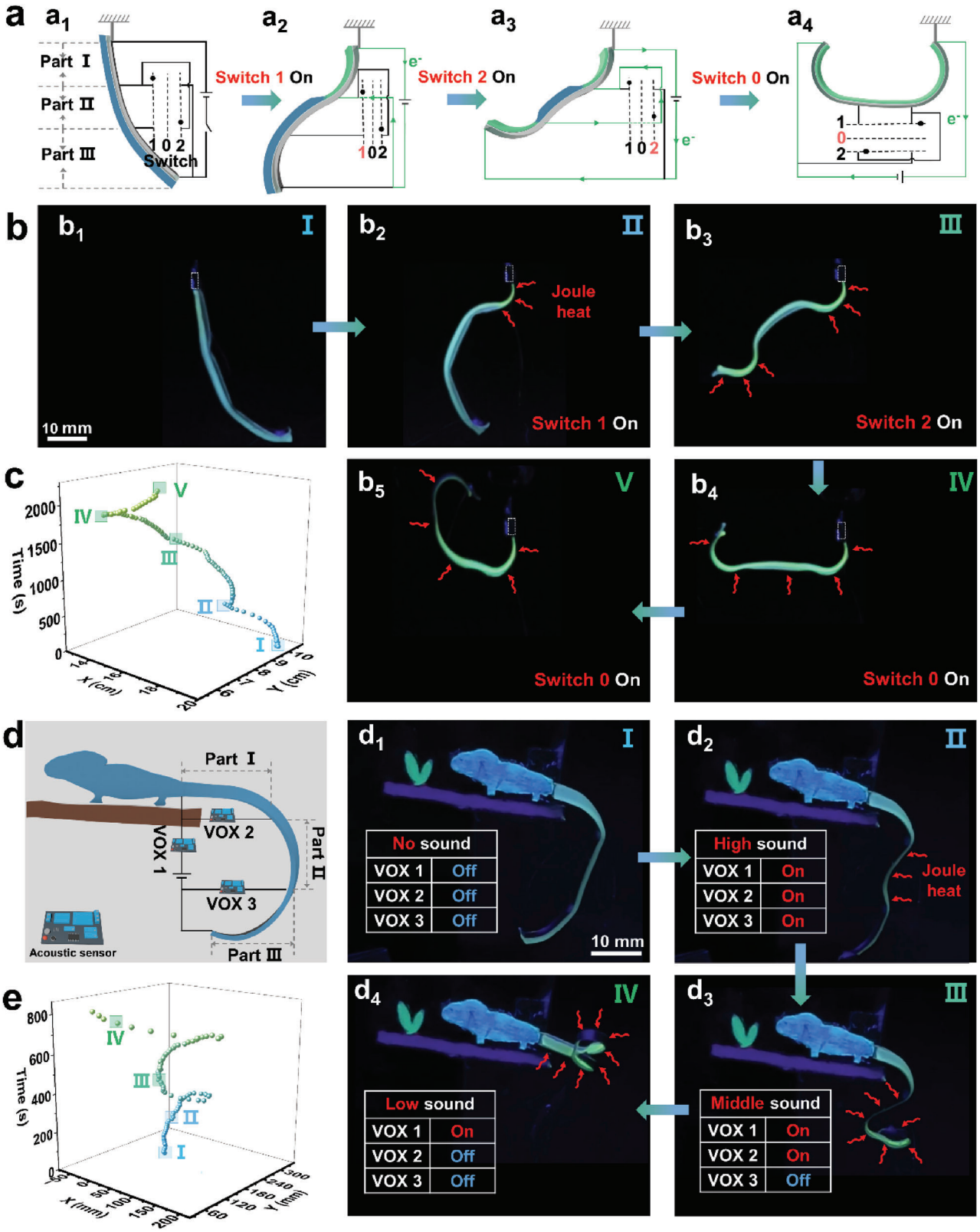


**Figure 4.** Demonstration of environment-interactive sequential soft actuators. a–c) Illustration (a) and photos (b) showing the local and sequential control over shape/color changes of different parts of the ECC actuator by hand-switching of the universal change-over switch (UCOS) under the input of 12 V, and the motion trajectory of its unfixed end (c). d,e) Illustration and photos showing environment-interactive artificial chameleon actuator that could intelligently sense the environmental sound signal change to adjust the actuating behaviors of its tail part under the input of 20 V, just like a real chameleon (d) and its motion trajectory (e). All photos were taken under a 365 nm UV lamp.

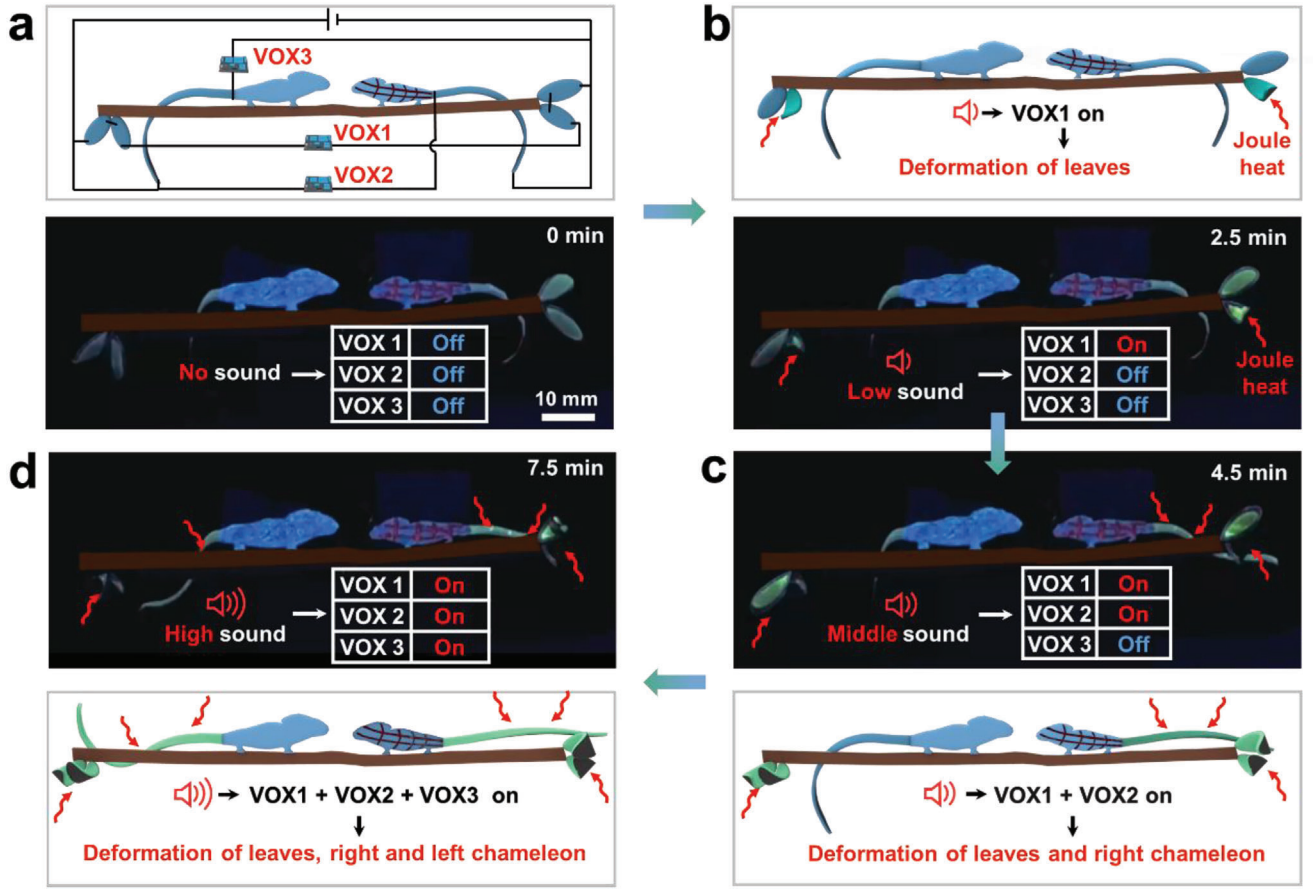


**Figure 5.** Demonstration of bio-inspired environment-interactive system. a–d) The illustration and photos showing the environment-interactive system with electrically (15 V) powered stepwise control over the color/shape changes of different parts upon reception of increasing environmental sound signals, no sound (a), low sound (b), middle sound (c) and high sound (d). All photos were taken under a 365 nm UV lamp.

synergistic shape/color changes in the tail part of the right chameleon actuator (Figure 5c). Successively, the left chameleon would curl its tail part when the environment sound was large enough to trigger the VOX3 switch (Figure 5d). In this way, the interesting environment sound interactive artificial systems were successfully accomplished by the joint use of our electrically powered actuators and commercial acoustic sensors (Movie S7, Supporting Information).

## 3. Conclusion

In summary, we reported a robust kind of bio-inspired electrically controlled fluorescence-color changeable hydrogel actuation system, which was prepared by the interfacial bonding of multicolor fluorescent PH3D hydrogel layer and conductive Graphene/PDMS film with electrocaloric effect. When applying voltage, graphene film rapidly completed electrothermal conversion and instantly transferred the Joule heat across PDMS to induce the shrinkage and blue-to-chartreuse color change of fluorescent hydrogel layer. This color-changing behavior is originated from the competition between PET process from DMAEMA to two fluorogens (DAEAN and DEAN), and AIE effect of these two fluorogens during dehydrating process. Based on this process, synergistic discoloration and deformation behavior of this hydrogel actuator was achieved. Besides, benefitting from the natural compatibility with existing electric devices and the facile controllability of electric signal, local and sequential actuation behavior was demonstrated by utilizing rational electric circuit and/or integrating with change-over switches. More importantly, an environment-interactive artificial chameleon that enabled programmable skin color and body shape upon different environment sounds were presented by joint use with the existing acoustic sensors. This work opened new avenues of color-changing soft actuators/robots and could provide an inspiration for developing functional integrated (e.g., human–robot interactive, environment-interactive) soft actuators/robots to extend the scope of applications.

## 4. Experimental Section

*Materials*: Acrylamide (AAm, 98.0%), acrylic acid (AAc, 98.0%), 2-Hydroxyethyl methacrylate (HEMA, 98%, stabilized by monomethyl ether hydroquinone), 2-(Dimethylamino)ethyl methacrylate (DMAEMA, 98%, stabilized by monomethyl ether hydroquinone), N,N′-Methylenebis(acrylamide) (Bis, 98.0%), ammonium peroxodisulfate (APS, ≥ 98.0%), benzophenone (BP, 99%) were purchased from Aladdin Chemistry Co. Ltd. 2-hydroxy-4′-(2-hydroxyethoxy)−2-methylpropiophenone (I2959, 98.0%) were obtained from TCI (Shanghai)

Development Co., Ltd. Graphene (GR, 5 wt %) was provided by Ningbo Morsh Technology Co., Ltd. DMSO (99%), ethanol (99%) were obtained from Sinopharm Chemical Reagent Co. Ltd. Acrylic acid-N-succinimide ester (AAc-NHS-ester, 90%) were purchased from Energy Chemical Co. Ltd. (NHS, 98%). PDMS films (250 mm × 200 mm × 200 µm) were purchased from Hangzhou Bald Advanced Materials Co. Ltd. The blue fluorescent monomer 4-(2-dimethylaminoethyloxy)-N-allyl-1,8-naphthalimide (DAEAN) and the yellow-green florescent monomer 4-(N,N-dimethylaminoethylene) amino-N-allyl-1,8-naphthalimide (DEAN) were synthesized according to the previous works.[25,31] HEMA and DMAEMA were passed through an alumina column to remove stabilizer before use. Other materials were used without further purification.

*Fabrication of the Poly(HEMA-DMAEMA-DAEAN-DEAN) (PH3D) Hydrogel*: The PH3D hydrogel was prepared by free radical copolymerization. Typically, DAEAN (fluorescent monomer, 5 mg) and DEAN (fluorescent monomer, 5 mg) were first dissolved in DMSO/$H_2O$ (5 mL/5 mL), followed by the addition of HEMA (monomer, 0.75 mL), DMAEMA ((monomer, 0.75 mL), and Bis (crosslinker, 15 mg). Next, the prepolymerization solution was pre-treated in refrigerator (4 °C) for 12 h. And then, fresh APS (initiator, 180 µL, 100 mg $mL^{-1}$) was added into 2 mL prepolymerization solution and rapidly transferred into the self-made mold with two quartz glass plates and a 0.5 mm thick silicon plate, whereafter copolymerization at 65 °C for 12 h to produce the gel. Finally, the as-fabricated gel was immersed in water to replace DMSO to give the PH3D hydrogel (PH3D).

*Growth of the Adhesive Layer on PDMS Film*: The growth method was inspired by previously reported works.[30] Specifically, 0.2 mm thick PDMS film was immersed in ethanol solution of BP (photo-initiator, 10 wt.%) for 12 h at room temperature to introduce BP into PDMS for further interfacial polymerization. Monomers AAc (0.16 mL), AAm (1.44 g), NHS (0.04 g), crosslinker Bis (0.002 g) and light initiator I2959 (0.08 g) were dissolved in 8 mL deionized $H_2O$, and then filtered with 0.45 µm syringe filters to get the precursor solution. Then, the PDMS containing BP and 0.3 mm thick silicon plate were successively placed on the quartz glass as a mold. The precursor solution was then added into the mold, followed by utilization of another quartz glass to seal the vessel for polymerization under ultraviolet light (5 W, 365 nm) for 2 h. After being dried at 60 °C for 30 min, the adhesive layer was grown on the PDMS surface.

*Fabrication of Graphene/PDMS*: The adhesive layer-functionalized PDMS film was cut into the designed shape and conformally placed on a glass substrate. The graphene film was fabricated according to the previous work.[29] Particularly, the graphene flakes were dispersed in anhydrous ethanol via ultrasonication for 6 h to obtain a 1.5 mg $mL^{-1}$ dispersion. Next, a specified volume of the as-fabricated dispersion was sprayed onto the standing water surface by a spray pot to form a uniform and ultra-thin graphene film on the water surface. Subsequently, a piece of microporous sponge was inserted into water along the wall of the vessel to break the equilibrium of the surface tension, resulting in the formation of a more compactly assembled graphene film. Finally, the as-prepared compact graphene film was transferred onto the surface of PDMS to obtain the Graphene/PDMS film.

*Preparation of Electrothermally fluorescence-Color Changeable (ECC) Hydrogel Actuator*: ECC actuator was prepared via facilely bringing the Graphene/PDMS film and the swollen fluorescent hydrogel together. Then, new covalent bonds were formed between the N-succinimide ester of the adhesive layer and the hydroxyl groups of fluorescent hydrogel, leading to the tight bonding of Graphene/PDMS film and fluorescent hydrogel sheet.

*Characterization*: The digital photos of fluorescence hydrogel and corresponding color-changing actuator were recorded under a UV lamp (ZF-5, 8 W, 365 nm) by a smart phone camera (IPHONE 13 pro). Steady-state fluorescence spectra were testified by a Hitachi F-4600 fluorescence spectrofluorometer equipped with a 150 W xenon lamp. Temperature-dependent FT-IR spectra were measured by Thermo Scientific Nicolet 6700 FT-IR spectrometer with a temperature control module. The characterization of micro morphology was conducted by a Hitachi S-4800 field-mission scanning electron microscope with an accelerating voltage of 5.0 kV. An Optris PI 400 IR thermal camera was used to capture the real-time surface temperature and IR images of the samples under different input voltages. PI connect software was employed for the analysis of these obtained data.

*Statistical Analysis*: The error bars of experimental data were presented as mean ± standard deviation (SD) with n = 3. Photos taken by mobile phone were processed by contrast and brightness in the article. Statistical analysis was carried out using the software of Excel. One-way analysis of variance (one-way ANOVA) was used to assess significant differences and the difference among samples was considered to be important when the calculated p-value was <0.05.

## Supporting Information

Supporting Information is available from the Wiley Online Library or from the author.

## Acknowledgements

This study was supported by National Natural Science Foundation of China (52073297), the Sino-German mobility programme (M-0424), Project of International Cooperation Foundation of Ningbo (2023H019), Zhejiang Provincial Natural Science Foundation of China (LR23E030001), Ningbo Natural Science Foundation (2021J194), Youth Innovation Promotion Association of Chinese Academy of Sciences (2019297).

## Conflict of Interest

The authors declare no conflict of interest.

## Data Availability Statement

The data that support the findings of this study are available from the corresponding author upon reasonable request.

## Keywords

electrothermal effect, environment-interaction, multicolor fluorescence, multilayer structures, polymeric hydrogels

Received: May 19, 2023
Revised: July 10, 2023
Published online:

[1] R. Hanlon, *Curr. Biol.* **2007**, *17*, R400.
[2] J. Teyssier, S. V. Saenko, D. van der Marel, M. C. Milinkovitch, *Nat. Commun.* **2015**, *6*, 6368.
[3] H. Vaknin, A. Bar-Akiva, R. Ovadia, A. Nissim-Levi, I. Forer, D. Weiss, M. Oren-Shamir, *Planta* **2005**, *222*, 19.
[4] a) D. Stuart-Fox, A. Moussalli, *Philos. Trans. R. Soc. Lond. B Biol. Sci.* **2009**, *364*, 463; b) S. Reiter, P. Hulsdunk, T. Woo, M. A. Lauterbach, J. S. Eberle, L. A. Akay, A. Longo, J. Meier-Credo, F. Kretschmer, J. D. Langer, M. Kaschube, G. Laurent, *Nature* **2018**, *562*, 361.
[5] a) J. Mu, G. Wang, H. Yan, H. Li, X. Wang, E. Gao, C. Hou, A. T. C. Pham, L. Wu, Q. Zhang, Y. Li, Z. Xu, Y. Guo, E. Reichmanis, H. Wang, M. Zhu, *Nat. Commun.* **2018**, *9*, 590; b) S. A. Morin, R. F. Shepherd, S. W. Kwok, A. A. Stokes, A. Nemiroski, G. M. Whitesides, *Science* **2012**, *337*, 828; c) W. Lu, M. Si, X. Le, T. Chen, *Acc. Chem. Res.* **2022**, *55*, 2291; d) Q. Zhao, Y. Wang, H. Cui, X. Du, *J. Mater. Chem. C* **2019**, *7*, 6493.

[6] a) Z. Zhang, Z. Chen, Y. Wang, J. Chi, Y. Wang, Y. Zhao, *Small Methods* **2019**, *3*, 1900519; b) Y. Yao, C. Yin, S. Hong, H. Chen, Q. Shi, J. Wang, X. Lu, N. Zhou, *Chem. Mater.* **2020**, *32*, 8868; c) X. Du, H. Cui, T. Xu, C. Huang, Y. Wang, Q. Zhao, Y. Xu, X. Wu, *Adv. Funct. Mater.* **2020**, *30*, 1909202; d) C. Yang, F. Su, Y. Xu, Y. Ma, L. Tang, N. Zhou, E. Liang, G. Wang, J. Tang, *ACS Macro Lett.* **2022**, *11*, 347; e) Y. Yang, F. Tian, X. Wang, P. Xu, W. An, Y. Hu, S. Xu, *ACS Appl. Mater. Interfaces* **2019**, *11*, 48428.

[7] H. Shang, X. Le, M. Si, S. Wu, Y. Peng, F. Shan, S. Wu, T. Chen, *Chem. Eng. J.* **2022**, *429*, 132290.

[8] a) X. Li, J. Liu, D. Li, S. Huang, K. Huang, X. Zhang, *Adv. Sci.* **2021**, *8*, 2101295; b) Y. Wang, H. Cui, Q. Zhao, X. Du, *Matter* **2019**, *1*, 626; c) H. Kim, H. Lee, I. Ha, J. Jung, P. Won, H. Cho, J. Yeo, S. Hong, S. Han, J. Kwon, K. J. Cho, S. H. Ko, *Adv. Funct. Mater.* **2018**, *28*, 1801847; d) C. Yang, B. Wu, J. Ruan, P. Zhao, L. Chen, D. Chen, F. Ye, *Adv. Mater.* **2021**, *33*, 2006361; e) Y.-S. Zhang, S. A. Jiang, J.-D. Lin, C. R. Lee, *J. Mater. Chem. C* **2020**, *8*, 5517; f) Z. Liu, H. Bisoyi, Y. Huang, M. Wang, H. Yang, Q. Li, *Angew. Chem., Int. Ed.* **2021**, *61*, e202115755; g) Y. Huang, H. K. Bisoyi, S. Huang, M. Wang, X. M. Chen, Z. Liu, H. Yang, Q. Li, *Angew. Chem., Int. Ed.* **2021**, *60*, 11247; h) R. Lan, Y. Gao, C. Shen, R. Huang, J. Bao, Z. Zhang, Q. Wang, L. Zhang, H. Yang, *Adv. Funct. Mater.* **2021**, *31*, 2010578.

[9] W. Wang, L. Yao, C.-Y. Cheng, T. Zhang, H. Atsumi, L. Wang, G. Wang, O. Anilionyte, H. Steiner, J. Ou, K. Zhou, C. Wawrousek, K. Petrecca, A. M. Belcher, R. Karnik, X. Zhao, D. I. C. Wang, H. Ishii, *Sci. Adv.* **2017**, *3*, e1601984.

[10] a) S. Guo, D. Wong, S. Wang, R. Gill, M. J. Serpe, *J. Mater. Chem. B* **2022**, *10*, 4416; b) C. Y. Li, D. Jiao, X. P. Hao, W. Hong, Q. Zheng, Z. L. Wu, *Adv. Mater.* **2023**, *35*, 2211802; c) X. Yu, Y. Cheng, H. Zhang, J. Zhang, M. Gao, C. Xu, B. Z. Tang, M. Zhu, *Nano Today* **2022**, *44*, 101502; d) R. Khodambashi, Y. Alsaid, R. Rico, H. Marvi, M. M. Peet, R. E. Fisher, S. Berman, X. He, D. M. Aukes, *Adv. Mater.* **2021**, *33*, 2005906; e) X. Liu, J. Liu, S. Lin, X. Zhao, *Mater. Today* **2020**, *36*, 102; f) B. B. Xu, Q. Liu, Z. Suo, R. C. Hayward, *Adv. Funct. Mater.* **2016**, *26*, 3218.

[11] a) A. K. Mishra, T. J. Wallin, W. Pan, P. Xu, K. Wang, E. P. Giannelis, B. Mazzolai, R. F. Shepherd, *Sci. Robot.* **2020**, *5*, eaaz3918; b) Q. L. Zhu, C. Du, Y. Dai, M. Daab, M. Matejdes, J. Breu, W. Hong, Q. Zheng, Z. L. Wu, *Nat. Commun.* **2020**, *11*, 5166; c) Y. S. Kim, M. Liu, Y. Ishida, Y. Ebina, M. Osada, T. Sasaki, T. Hikima, M. Takata, T. Aida, *Nat. Mater.* **2015**, *14*, 1002.

[12] a) Y. Ma, M. Hua, S. Wu, Y. Du, X. Pei, X. Zhu, F. Zhou, X. He, *Sci. Adv.* **2020**, *6*, eabd2520; b) Y. Cui, D. Li, C. Gong, C. Chang, *ACS Nano* **2021**, *15*, 13712.

[13] Y. Gao, L. Yu, J. C. Yeo, C. T. Lim, *Adv. Mater.* **2020**, *32*, 1902133.

[14] F. Fu, L. Shang, Z. Chen, Y. Yu, Y. Zhao, *Sci. Robot.* **2018**, *3*, eaar8580.

[15] Z. Li, P. Liu, X. Ji, J. Gong, Y. Hu, W. Wu, X. Wang, H. Q. Peng, R. T. K. Kwok, J. W. Y. Lam, J. Lu, B. Z. Tang, *Adv. Mater.* **2020**, *32*, 1906493.

[16] C. Ma, W. Lu, X. Yang, J. He, X. Le, L. Wang, J. Zhang, M. J. Serpe, Y. Huang, T. Chen, *Adv. Funct. Mater.* **2018**, *28*, 1704568.

[17] a) S. Wei, W. Lu, X. Le, C. Ma, H. Lin, B. Wu, J. Zhang, P. Theato, T. Chen, *Angew. Chem., Int. Ed.* **2019**, *58*, 16243; b) S. Wu, H. Shi, W. Lu, S. Wei, H. Shang, H. Liu, M. Si, X. Le, G. Yin, P. Theato, T. Chen, *Angew. Chem., Int. Ed.* **2021**, *60*, 21890.

[18] S. Wei, H. Qiu, H. Shi, W. Lu, H. Liu, H. Yan, D. Zhang, J. Zhang, P. Theato, Y. Wei, T. Chen, *ACS Nano* **2021**, *15*, 10415.

[19] X. Le, W. Lu, J. Zhang, T. Chen, *Adv. Sci.* **2019**, *6*, 1801584.

[20] a) T. Kuriyama, K. Miyaji, M. Sugimoto, M. Hasegawa, *Zool. Sci.* **2006**, *23*, 793; b) R. A. Ligon, K. J. McGraw, *Biol. Lett.* **2013**, *9*, 20130892; c) R. Bickel, J. B. Losos, *Biol. J. Linn. Soc. Lond.* **2002**, *76*, 91.

[21] a) C. Wang, K. Sim, J. Chen, H. Kim, Z. Rao, Y. Li, W. Chen, J. Song, R. Verduzco, C. Yu, *Adv. Mater.* **2018**, *30*, 1706695; b) Y. Ling, W. Pang, X. Li, S. Goswami, Z. Xu, D. Stroman, Y. Liu, Q. Fei, Y. Xu, G. Zhao, B. Sun, J. Xie, G. Huang, Y. Zhang, Z. Yan, *Adv. Mater.* **2020**, *32*, 1908475.

[22] a) R. Wang, Y. Zhang, W. Lu, B. Wu, S. Wei, S. Wu, W. Wang, T. Chen, *Angew. Chem., Int. Ed.* **2023**, *62*, e202300417; b) S. Wei, W. Lu, H. Shi, S. Wu, X. Le, G. Yin, Q. Liu, T. Chen, *Adv. Mater.* **2023**, *35*, 2300615.

[23] S. Wu, H. Shi, S. Wei, H. Shang, W. Xie, X. Chen, W. Lu, T. Chen, *Small* **2023**, *19*, 2300191.

[24] a) J. C. Zhu, T. Han, Y. Guo, P. Wang, H. L. Xie, Z.-G. Meng, Z.-Q. Yu, B. Z. Tang, *Macromolecules* **2019**, *52*, 3668; b) Y. Tian, M. Li, Y. Liu, *Molecules* **2020**, *25*, 4465; c) H. Liu, Y. Fu, W. Xu, Q. He, H. Cao, G. Liu, J. Cheng, *Sci. China Chem.* **2018**, *61*, 857.

[25] P. Li, D. Zhang, Y. Zhang, W. Lu, J. Zhang, W. Wang, Q. He, P. Théato, T. Chen, *ACS Macro. Lett.* **2019**, *8*, 937.

[26] J. Cao, C. Lu, J. Zhuang, M. Liu, X. Zhang, Y. Yu, Q. Tao, *Angew. Chem., Int. Ed.* **2017**, *56*, 8795.

[27] K. Gong, L. Hou, P. Wu, *Adv. Mater.* **2022**, *34*, 2201065.

[28] L. Wang, X. Zhang, Y. Xia, X. Zhao, Z. Xue, K. Sui, X. Dong, D. Wang, *Adv. Mater.* **2019**, *31*, 1902381.

[29] S. Wang, Y. Gao, A. Wei, P. Xiao, Y. Liang, W. Lu, C. Chen, C. Zhang, G. Yang, H. Yao, T. Chen, *Nat. Commun.* **2020**, *11*, 4359.

[30] a) H. Yuk, C. E. Varela, C. S. Nabzdyk, X. Mao, R. F. Padera, E. T. Roche, X. Zhao, *Nature* **2019**, *575*, 169; b) Y. Yu, H. Yuk, G. A. Parada, Y. Wu, X. Liu, C. S. Nabzdyk, K. Youcef-Toumi, J. Zang, X. Zhao, *Adv. Mater.* **2019**, *31*, 1807101.

[31] H. Qiu, S. Wei, H. Liu, B. Zhan, H. Yan, W. Lu, J. Zhang, S. Wu, T. Chen, *Adv. Intell. Syst.* **2021**, *3*, 2000239.